Arabian Journal of Chemistry (2023) **16**, 104446

King Saud University

**Arabian Journal of Chemistry**

www.ksu.edu.sa
www.sciencedirect.com

ORIGINAL ARTICLE

# Effect of Coriolis and buoyancy forces on three-dimensional flow of chemically reactive tangent hyperbolic fluid subject to variable viscosity

**T. Salahuddin** [a], **Moeen Taj** [a], **K. Ayoub** [a], **Mair Khan** [b,*]

[a] *Department of Mathematics, Mirpur University of Science and Technology, Mirpur 10250, Azad Kashmir, Pakistan*
[b] *Department of Mathematics, University College of Zhob, BUITEMS, Zhob 85200, Pakistan*

Received 9 June 2022; accepted 17 November 2022
Available online 13 December 2022

**KEYWORDS**

Coriolis and buoyancy forces;
Thermo-migration of nano-sized particles- thermophoresis;
Haphazard motion of nano-sized particles-Brownian motion of particles;
Viscosity;
Rotatory fluid;
Activation energy

**Abstract** Thermophoresis effect has wide range of applications in electro-static precipitators and in biology for calculating single biological macro molecules, such as genomic-length DNA and HIV virus in the micro channels. Current study deal with effects of Coriolis and buoyancy forces on the three-dimensional boundary layer flow of tangent hyperbolic fluid with thermo-migration and haphazard motion of nano-sized particles. Arrhenius kind of chemical reaction is taken along an exponentially stretchable surface. The main focus of current exploration is to execute shear thinning nano-liquid flow past an exponentially rotating stretchable surface under the influence of variable viscosity, mixed convection and activation energy. We are motivated to explore the features of three-dimensional shear thinning model combined under the features of mixed convention, variable viscosity, and activation energy. The mathematical model is designed to generate PDEs and converted them into ODEs by employing fractious transformation. The numerical outcomes are exhibited via graphs by employing Bvp4c numerical technique whereas the values of skin friction coefficient are calculated by monopolizing shooting method. Characteristics of the parameters appearing in modeling like the viscosity parameter, power-law index, local Weissenberg number, mix convection parameter, rotation parameter, Prandtl number and chemical reaction parameter are comprehensively analyzed through graphical behavior. The impact of governing parameters on skin friction, heat and mass transfer rates is illustrated through tables. The detail analysis anticipates that the elevation in Weissenberg number and porosity caused decline in velocity. Further, the temperature behaves doppositely analogous to development Prandtl besides the thermophoresis parameter.


* Corresponding author.
E-mail address: mair.khan@math.qau.edu.pk (M. Khan).
Peer review under responsibility of King Saud University.

Production and hosting by Elsevier

https://doi.org/10.1016/j.arabjc.2022.104446
1878-5352 © 2022 Published by Elsevier B.V. on behalf of King Saud University.

## 1. Introduction

Buoyancy is the force that causes the object to float. It is a force that applied to an object that is partially or completely immersed in the liquid. Differences in the pressure exerted on the opposing side of an object immersed in a statics fluid causes buoyancy force. It is also known as buoyant force. Coriolis force is an inertial or frictional force that acts on objects that are in motion within a frame of reference that rotates with respect to an inertial frame. Shah et al. (Nehad Ali Shah) deliberated the significance of Grashof number on the flow of fluid under the influence of free convection and mixed convection. Bellahsen et al. (Bellahsen et al., 2013) studied the role of buoyancy forces arising from thickness variations in the lithosphere during rifting. Amahmid et al. (Amahmid et al., 1999) examined the existence of boundary layer flow induced by opposing buoyancy effects in a vertical slot. Chang et al. (Woei Chang, 2010) investigated the rotating buoyancy and Coriolis effects on the detailed Nu distributions above the leading and trailing ribbed walls of a square sectioned. Hallan et al. (Hallan and Rana, 2001) explored the impact of perturbation on Coriolis and centrifugal forces in Robe's circular restricted by three body problem with different densities on the equilibrium point by different methods. Animasaun et al. (Animasaun et al., 2020) investigated the importance of buoyancy forces and thickness of paraboloid revolution on the dynamics of Erying-Powell liquid subject to equal diffusivity. Gong et al. (Gong et al., 2018) inspected the joined effects of Coriolis force and temperature viscosity transmission of rotating hydro-viscous film. Riahi et al. (Riahi, 2001) revealed the effects of inclined rotation on chimney convection, under the external barrier of a strong magnetic field.

Tangent hyperbolic fluid is a pseudo-plastic fluid model that relates the shear thinning phenomenon which has numerous properties from viscous and ideal plastic fluids etc. Nadeem et al. (Nadeem, 2010) inspected the effect of temperature dependent viscosity and magnetic impact on the peristaltic flow of an incompressible Newtonian fluid. The effect of thermophoresis and Brownian motion or tangent hyperbolic nanofluid was executed by Salahuddin et al. (Salahuddin et al., 2017). Shahzad et al. (Shahzad et al., 2019) described the heat effects on hyperbolic tangent fluid. Impact of magnetic flux with suction injection on hyperboloid tangent fluid was investigated by Ullah et at. (Ullah et al., 2020). Abegunrin et al. (Abegunrin et al., 2016) investigated the motion of Williamson and Casson fluids over a horizontal surface of a paraboloid revolution in the existance of non-linear thermal radiation. In the presence of buoyancy and partial slip the rotation of Williamson liquid over a horizontal surface of a paraboloid of revolution was investigated by Abegunrin et al. (Abegunrin and Animasaun, 2017). Khan et al. (Mair Khan et al., 2018) examined the impact of variable viscosity and dual stratification on Williamson fluid flow past a nonlinear stretchable sheet. Nagendramma et al. (Nagendramma et al., 2018) investigated the shear thinning fluid in the presence of temperature source near a stretching cylinder in permeable space. Hayat et al. (Hayat et al., 2018) evaluated the peristaltic transport of tangent hyperbolic liquid in an inclined channel. Atif et al. (Atif et al., 2019) studied the magnetic hydrodynamic shear thinning nanoparticles over a stretchable surface in the existence of viscid dissipation, thermal conductivity and thermal radiation. Petrolo et al. (D. Petrolo) detected the theoretical analysis in Rayleigh-Benard convection of a non-Newtonian power law fluid within a vertical permeable layer heated from below.

Thermophoresis is a phenomenon observed in the mobile particles where different types of particles react differently. The term thermophoresis is most applicable to aerosol mixture, the term soret effect generally applies to the liquid mixture, which behaves differently. Wakif et al. (Wakif) explored the importance of nanoparticles due to thermopheratic force on the *meta*-analysis in presence of temperature gradient. El-Sapa et al. (El-Sapa, 2020) studied the effect of permeability of the permeable medium on thermophoretic velocity of the confined particle. Chernyak et al. (Chernyak and Sograbi, 2019) scrutinized the thermal polarization of an aerosol particle along with the force of thermophoresis under the influence of free molecules. Ullah et al. (Ullah, 2018) imitated the influence of electrically conducting mixed convection flow of Casson nano-fluid generated by a moving wedge in the presence of thermal radiation. Shah et al. (Shaha, 2018) studied the 3D third grade nanofluid flow in a rotating system over a semi-infinite porous inclined flat plate in the existence of thermophoresis and non-uniform heat source/sink. Ramachandran et al. (Ramachandran et al., 2020) detected the molecular dynamics simulation to obtain the effects of the particle shape, size and orientation on thermophoresis in nanofluids. Hassan et al. (Hassan, 2019) explored the significance of internal heat source on variable viscosity with the reaction of Couette fluid by considering the velocity of upper plate as constant while lower plate was stationary. Bhatti at al. (Bhatti et al., 2016) analyzed the simultaneous effects of thermal transfer which involves the blood flow along variable viscosity accumulating with the peristaltic transport of bloodstream particles. Hadji et al. (Hadji et al., 2020) determined the thermal conductivity of traditional building materials obtained by mixing of two kinds of soil, agricultural and soil taken from the desert land.

The Brownian motion is named after Botanist Robert Brown who firstly observed it in 1827, particles of both liquids and gases move randomly. Large particles can be transported by lighter fast-moving molecules named as Brownian motion. Mittal et al. (Akhil, 2020) evaluated 2D mixed convective magneto-hydrodynamic stagnation point flow of Casson liquid over an infinite plate in permeable medium. Animasaun et al. (Animasauna et al., 2019) examined the *meta*-analysis on the growth of nano-sized particles with other physical properties of liquid. Pei et al. (Pei et al., 2020) explored the averaging principle for time dependent and stochastic differential equations determined by fractional Brownian motion and standard Brownian motion (SBM). Dogonchi et al. (Dogonchi and Seyyedi, 2019) evaluated the magnetic nano liquid natural convection in the permeable enclosure by Brownian motion using the control volume finite element method. And also discussed the feature of Darcy number, Rayleigh number and angle of magnetic field parameter. Harish et al. (Harish) discussed the thermal performance of metallic and ceramic nano-fluids in the influence of turbulent flow conditions. Wang et al. (Kaidi Wang et al., 2020) inspected the non-Kolmogorov atmospheric turbulence phase screen by using (IE-FB) method. Some advantageous studies relevant to current exploration have been reported as (Ahmad et al., 2014; Khan et al., 2014; Mustafa et al.; Khan et al., 2015; Ali et al., 2021; Khan and Nadeem, 2021; Wang et al., 2022; Wakif et al., 2020; Shamshuddin and Satya Narayana, 2020; Venkateswarlu and Satya Narayana, 2021; Naidu et al., 2021; Satya Narayana et al., 2021; Satya Narayana et al., 2021; Katam et al., 2021; Bashir et al., 2022).

The Principal objective of current study is to investigate the shear thinning nano-fluid model near an exponentially rotating stretched surface with the effects of mixed convection, variable viscosity and heat generation. From the previous investigation, it has been analyzed that the scholars have not yet discussed the shear thinning fluid model in three-dimensional space. The 2-D flow of shear thinning Williamson fluid was analyzed by Salahuddin et al. (Salahuddin, 2019) by employing the characteristics of Cattaneo Christov heat and mass flux models with temperature dependent viscosity. Therefore, we are motivated to investigate the impact of mixed convention, variable viscosity and activation energy on three-dimensional shear thinning fluid model near 3D stretched surface. The given equations are generated in the form of ODEs and solved numerically by bpv4c using matlab. Furthermore, the graphs are drawn to check the behavior of velocity, temperature, and concentration profiles for 3D tangent hyperbolic model. The governing results are calculated through graphs. To the best of our knowledge and understanding, the achieved numerical solutions employing the current suggested model for tangent hyperbolic fluid set a novel scope for scholars in the analysis of heat transfer.

## 2. Mathematical formulation

We assume steady incompressible 3D flow of shear thinning nano-fluid with the effects of mixed convection, time dependent viscosity and heat generation (Fig. 1). Cartesian coordinate system is considered in which sheet is placed in xy-plane and flow is along $z$ direction with $z \geq 0$.

Suppose that the given surface is stretchable in plane with velocity $U = U_0 e^{\frac{x}{L}}$ and the shear thinning nanofluid rotates with constant rate $\Omega$ along z-axis.

$$\nabla . V = 0, \tag{1}$$

$$\rho\left[\frac{dV}{dt} + \left(2\bar{\Omega}\times V\right) + \left(\bar{\Omega}\times\left(\bar{\Omega}\times V\right)\right)\right] = \nabla.\tau, \tag{2}$$

$$(\rho C)_p \frac{dT}{dt} = k\nabla^2 T + (\rho C)_f\left[D_B \nabla C.\nabla T + \frac{D_T}{T_\infty}\left(\nabla T^2\right)\right], \tag{3}$$

$$\frac{dC}{dt} = D_B\nabla^2 C - K_r{}^2\left(\frac{T}{T_\infty}\right)^n e^{\frac{-E_a}{KT}}(C - C_\infty) + \frac{D_T}{T_\infty}\left(\nabla^2 T\right), \tag{4}$$

where k is thermal conductivity, $V$ is vector of velocity, $\bar{\Omega} = [0, 0, \bar{\Omega}]$ is the vector of angular velocity, $(\rho C)_p$ mentions the effective heat capacity of shear thinning nanofluid, $\rho$be the density of liquid, $D_B$is the coefficient of Brownian motion, $K_r{}^2$ is chemical reaction rate constant,$D_T$ is coefficient of thermophoretic diffusion, $(\rho C)_p$effective heat capacity of the base fluid, $\left(\frac{T}{T_\infty}\right)^n e^{\frac{-E_a}{KT}}(C - C_\infty)$is the Arrhenius function, n is the constant of exponent and $E_a$ is the activation energy.

Where the Cauchy stress tensor $\bar{\tau}$ for tangent hyperbolic fluid model is defined as:

$$\bar{\tau} = -pI + \boldsymbol{S}, \tag{5}$$

in above expression $S$ is extra stress tensor of tangent hyperbolic fluid delineated as:

$$\boldsymbol{S} = \mu_\infty + (\mu_0 - \mu_\infty)tanh(\Gamma\dot{\gamma})^n]B_1, \tag{6}$$

here $\mu_\infty$ is limiting viscosity shear rate, $\mu_\infty$ is limiting viscosity zero shear rate, $\Gamma$ is time dependent constant, n is flow behavior index, $B_1$ is the first Rivilin Ereckson tensor and $\dot{\gamma}$ is defined as

$$\dot{\gamma} = \frac{\sqrt{trcB_1{}^2}}{2} \tag{7}$$

The pertinent equations for energy, momentum and concentration equations according to the stated restrictions for fluid flow are given as:

$$u_x + u_y + u_z = 0, \tag{8}$$

$$uu_x + vu_y + wu_z - 2\bar{\Omega}v = \frac{1-n}{\rho}\frac{\partial}{\partial z}(\mu(T)u_z) + \frac{n\Gamma}{\rho\sqrt{2}} \times \frac{\partial}{\partial z}\left(\mu(T)(u_z)\{u_z^2 + v_z^2\}^{0.5}\right) - g[(T - T_\infty)B_T + (C - C_\infty)B_C], \tag{9}$$

$$uv_x + vv_y + wv_z + 2\bar{\Omega}u = \frac{1-n}{\rho}\frac{\partial}{\partial z}(\mu(T)v_z) + \frac{n\Gamma}{\rho\sqrt{2}} \times \frac{\partial}{\partial z}\left(\mu(T)(v_z)\{u_z^2 + v_z^2\}^{0.5}\right), \tag{10}$$

$$uT_x + vT_y + wT_z = \alpha T_{zz} + \tau\left[D_B\frac{\partial T}{\partial x}\frac{\partial C}{\partial x} + \frac{D_T}{T_\infty}\left(\frac{\partial T}{\partial z}\right)^2\right], \tag{11}$$

$$uC_x + vC_y + wC_z = D_B C_{zz} - K_r{}^2\left(\frac{T}{T_\infty}\right)^n e^{\frac{-E_a}{KT}}(C - C_\infty) + \frac{D_T}{T_\infty}\frac{\partial^2 T}{\partial z^2}, \tag{12}$$

and the associated boundary conditions are.

$$u = U_w = u_0 e^{\frac{x}{L}},\ v = 0,\ w = 0,\ T = T_w,\ C = C_w \text{ at } z = 0,$$
$$u = 0,\ v \to 0,\ T \to T_\infty,\ C \to C_\infty \text{ as } z \to \infty. \tag{13}$$

Eqs. (8)–(12) with boundary conditions (13) reduce to ODES by using these variables:

$$\eta = \sqrt{\frac{u_0}{2\nu L}}e^{\frac{x}{2L}}z,\ u = u_0 e^{\frac{x}{L}}f'(\eta),\ v = u_0 e^{\frac{x}{L}}g(\eta),$$
$$w = -\sqrt{\frac{\nu u_0}{2L}}e^{\frac{x}{2L}}\left(f(\eta) + \eta f'(\eta)\right),\ T = T_\infty + T_0 e^{\frac{x}{2L}}\theta,\ C = C_\infty + C_0 e^{\frac{x}{2L}}\phi, \tag{14}$$

The equation of continuity (8) is satisfied in the view of (14), our reaming equations become:

$$(1 - A\theta)\{(1-n)f + \tfrac{n}{2}Wef''(f'^2 + g'^2)^{0.5} + \tfrac{n}{2}We\left(\tfrac{(f'f''' + g'g'')f''}{(f'^2+g'^2)^{0.5}}\right)\}$$
$$+(1 - A\theta)A\theta'\{(1-n)f'' + \tfrac{n}{2}Wef''(f'^2 + g'^2)^{0.5}\} - 2f'^2 hfill$$
$$+2ff'' + 4\Omega g + 2\beta\theta + 2\gamma\phi = 0, \tag{15}$$

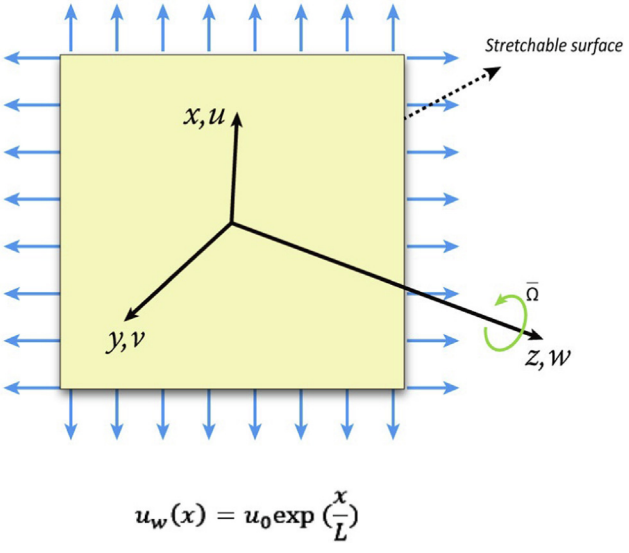


**Fig. 1** Physical configuration and Cartesian coordinate system.

$$(1-A\theta)\{(1-n)g''+\tfrac{n}{2}Weg''(f'^2+g'^2)^{0.5}+\tfrac{n}{2}We(\tfrac{(g'g''+f'f''')g'}{(f'^2+g'^2)^{0.5}})\}$$
$$+(1-A\theta)A\theta'\{(1-n)g'+\tfrac{n}{2}Weg'(f'^2+g'^2)^{0.5}\}$$
$$-2f'g+2fg'-4\Omega f'=0, \tag{16}$$

$$\frac{1}{\Pr}\theta''+f\theta'+N_b\theta'\varphi'+N_t\theta'^2=0, \tag{17}$$

$$\varphi''+Scf\varphi'+\left(\frac{N_t}{N_b}\right)\theta''-Sc\lambda(1-n\delta\theta)e^{\frac{E}{1+\delta\theta}}\varphi=0, \tag{18}$$

the boundary conditions become:

$$f=g=0,\ f'=1,\ \theta=\phi=1 \text{ at } \eta=0, f'\to 0,\ g\to 0,\ \theta\to 0,\ \phi\to 0 \text{ as } \eta\to\infty. \tag{19}$$

Now we define local skin friction coefficients, representing drag coefficients at the surface are

$$C_{f_x}=\frac{\tau_{zx}|_{z=0}}{\frac{1}{2}\rho u_w^2}, C_{f_y}=\frac{\tau_{zy}|_{z=0}}{\frac{1}{2}\rho u_w^2}, \tag{20}$$

now using Eq. (14) in (20), we obtain the following form:

$$\sqrt{2}C_{fx}\mathrm{Re}_x^{\frac{1}{2}}=(1-A\theta(0))f''(0)[(1-n)+\tfrac{We}{\sqrt{2}}\left\{f''(0))^2+(g'(0))^2\right\}^{\frac{1}{2}}],$$
$$\sqrt{2}C_{fy}\mathrm{Re}_y^{\frac{1}{2}}=(1-A\theta(0))g'(0)[(1-n)+\tfrac{We}{\sqrt{2}}\left\{f''(0))^2+(g'(0))^2\right\}^{\frac{1}{2}}], \tag{21}$$

Other significant physical quantities like Nusselt number $Nu_x$ and the Sherwood number $Sh_x$ are:

$$Nu_x=\frac{xq_w}{k(T_w-T_\infty)}, Sh_x=\frac{xq_m}{D(C_w-C_\infty)}, \tag{22}$$

now using Eq. (14) in (22), we get:

$$Nu_x\frac{L}{x}\sqrt{\frac{2}{\mathrm{Re}_x}}=-\theta'(0), Sh_x\frac{L}{x}\sqrt{\frac{2}{\mathrm{Re}_x}}=-\phi'(0). \tag{23}$$

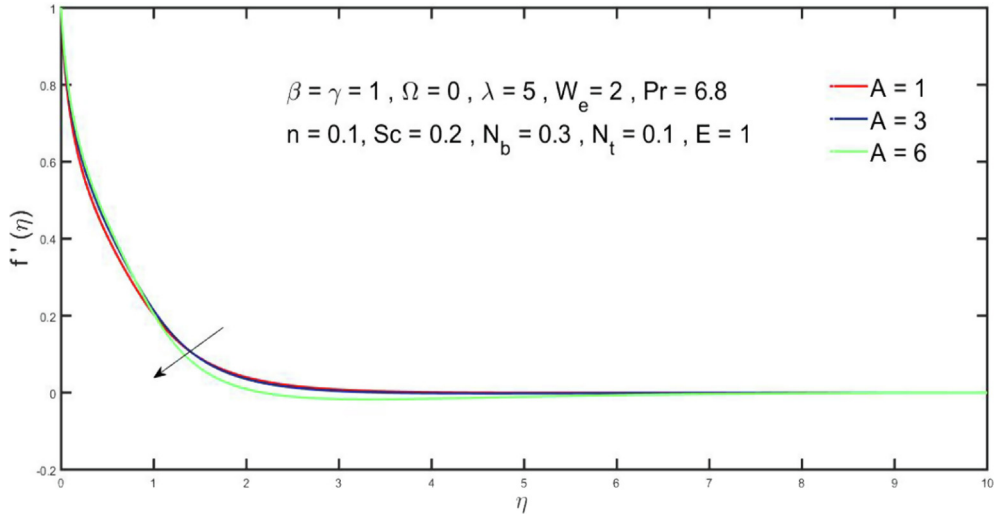


**Fig 2** Effect of $A$ on $f'(\eta)$.

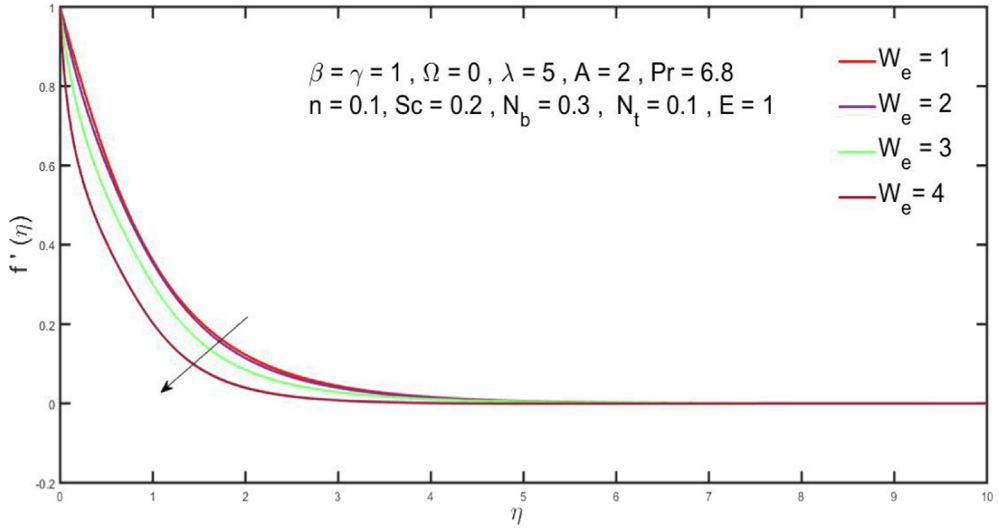


**Fig 3** Effects of $W_e$ on $f'(\eta)$.

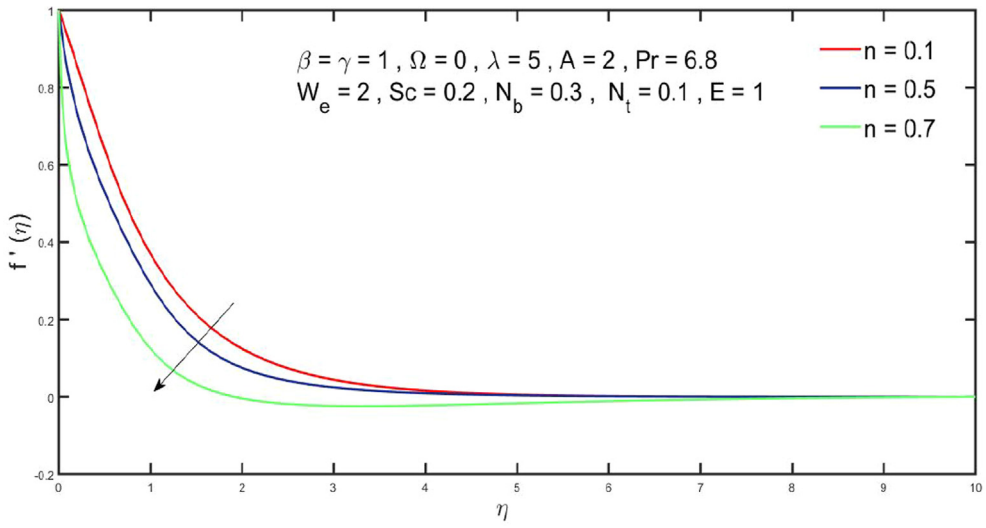


**Fig 4** Influence of $n$ on $f'(\eta)$.

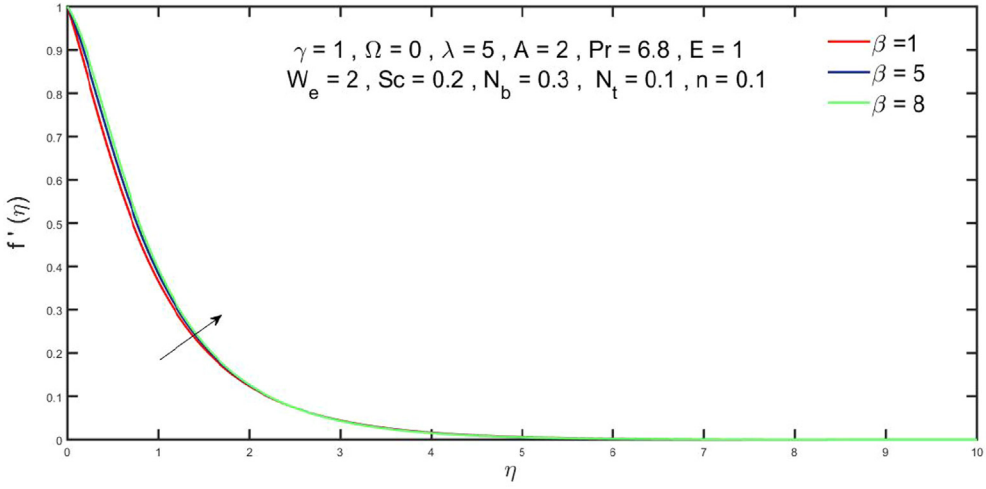


**Fig 5** Influence of $\beta$ on $f'(\eta)$.

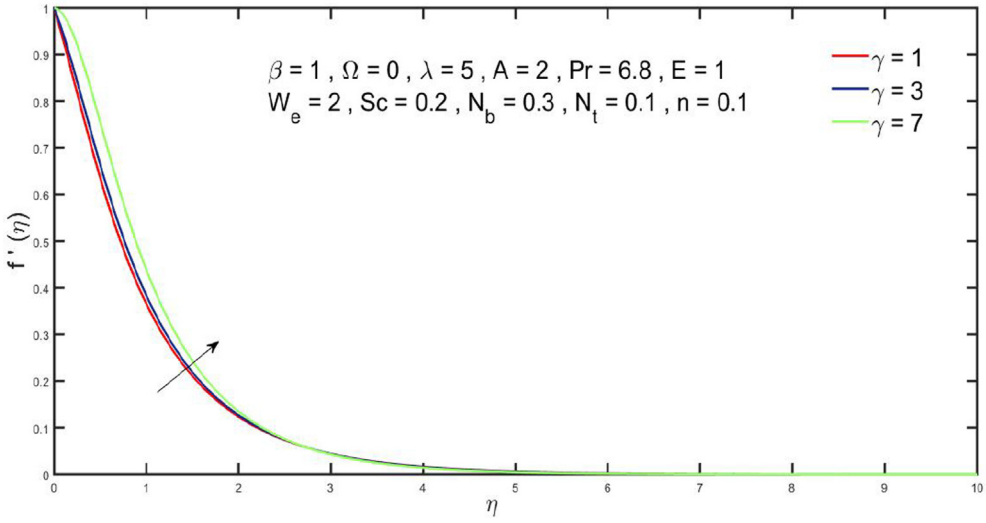


**Fig 6** Effects of $\gamma$ on $f'(\eta)$.

In Eqs. (15)–(18), Ω is the rotational parameter, buoyancy parameter is $\gamma$, $N_t$ denotes thermophoresis parameter, $We$denotes Weissengnberg number, chemical reaction rate parameter is $\lambda$, Pr denotes as Prandtl number, variable viscosity parameter $A$, mixed convection parameter $\beta$, $Sc$ denotes the Schmidt number, $N_b$denotes the Brownian diffusion parameter and $E$ is the activation energy. These parameters are given below:

$$\Omega=\frac{L\bar{\Omega}}{u_w}, Sc=\frac{\nu}{D_B}, Pr=\frac{\nu}{\alpha}, N_b=\frac{\tau D_B C_0}{\nu}, N_b=\frac{\tau D_T T_0}{\nu T_\infty}, We=u_0\sqrt{\frac{u_0}{\nu L}}\Gamma e^{\frac{3x}{2l}},$$
$$\beta=\frac{gLB_T T_0}{{u_0}^2}e^{-\frac{3x}{2l}}, \gamma=\frac{gLB_C C_0}{{u_0}^2}e^{-\frac{3x}{2l}}, A=-\xi(T_s-T_0), E=\frac{-E_a}{KT_\infty}, \lambda=\frac{2{K_r}^2 L}{u_0}. \tag{24}$$

Where the dimension of rotational parameter Ω, thermophoresis parameter $N_t$ and Weissengnberg number $We$ are given below:

$$\Omega=\frac{LT^{-1}}{LT^{-1}}, N_t=\frac{\frac{LTKML^2}{LTTKM}}{\frac{L^2}{K}}, We=\frac{TL}{T}\sqrt{\frac{\frac{L}{T}}{\frac{L^2 L}{T}}}. \tag{25}$$

## 3. Numerical solution

The momentum equations (15) and (16), temperature equation (17) and concentration equation (18) along with appropriate boundary conditions (19) are numerically determined by using Bvp4c Matlab software for different values of flow parameters. This method configures higher order finite difference method that uses collocation method which includes the three-stage Lobatto IIIa technique with forth-order accuracy. This technique converts the ODEs into set of first order differential equations. In order to reduce Eqs. (15)–(18) into the system of first order differential equations, we substitute

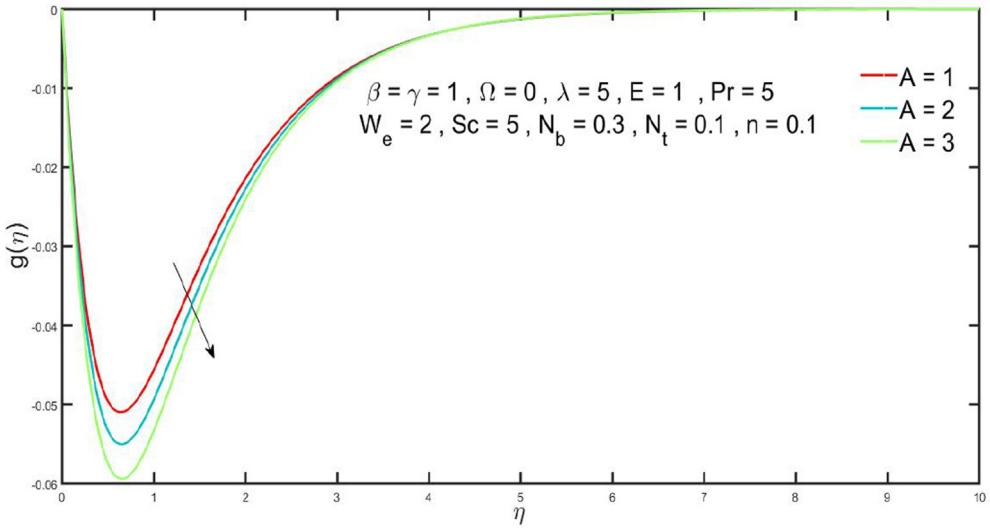


**Fig 7** Effects of $A$ on $g(\eta)$.

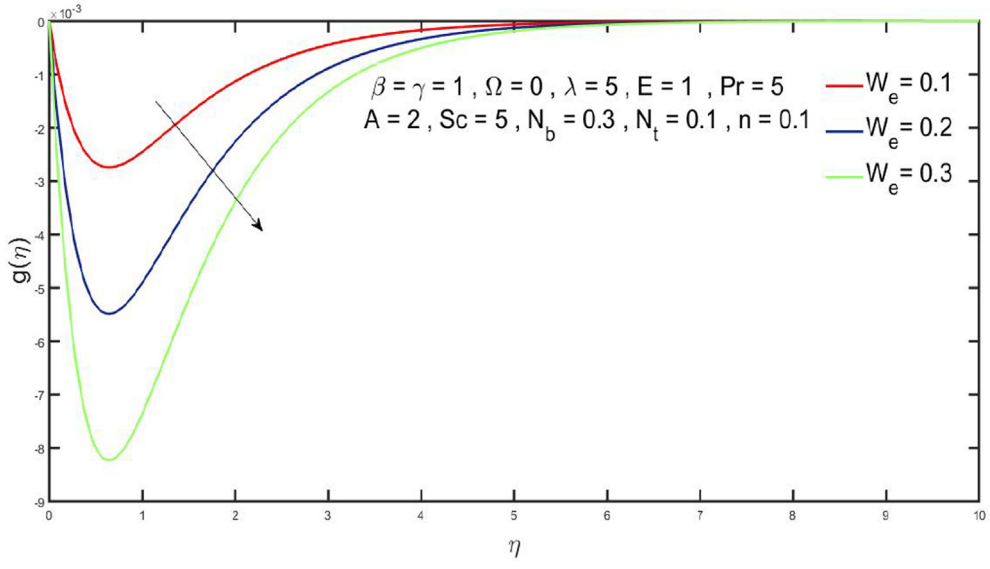


**Fig 8** Effect of $W_e$ on $g(\eta)$.

$$y_1 = f, y_2 = f\prime, \quad y_3 = f\prime\prime, \quad y_4 = g, y_5 = g\prime, \\ y_6 = \theta, y_7 = \theta', y_8 = \varphi, y_9 = \varphi\prime, \tag{26}$$

$$f''' \left[ (1-n) + \frac{nWe(f''^2 + g'^2)^{0.5}}{2} + \frac{nWef''^2}{2(f''^2 + g'^2)^{0.5}} \right] \\ = \frac{2f'^2}{1-A\theta} - \frac{2ff''}{1-A\theta} - \frac{4\Omega g}{1-A\theta} - \frac{2\beta\theta}{1-A\theta} - \frac{2\gamma\varphi}{1-A\theta} \\ - \frac{nWef'g''}{2(f''^2 + g'^2)^{0.5}} - A\theta' f''(1-n) \\ - \frac{A\theta' nWef''}{2}(f''^2 + g'^2)^{0.5}, \tag{27}$$

$$g'' \left[ (1-n) + \frac{nWe(f''^2 + g'^2)^{0.5}}{2} + \frac{nWeg'^2}{2(f''^2 + g'^2)^{0.5}} \right] \\ = \frac{2f'g}{1-A\theta} - \frac{2fg'}{1-A\theta} + \frac{4\Omega f}{1-A\theta} - \frac{nWegf''f'''}{2(f''^2 + g'^2)^{0.5}} \\ - A\theta' g'(1-n) - \frac{A\theta' nWeg'}{2}(f''^2 + g'^2)^{0.5}, \tag{28}$$

$$\theta'' = -Prf\theta' - PrN_b\theta'\phi' - PrN_t\theta'^2 \tag{29}$$

$$\varphi'' = Sc\lambda(1 - n\delta\theta)e^{\frac{E}{1+\delta\theta}} - Scf\varphi' - \frac{N_t}{N_b}\theta'', \tag{30}$$

and the boundary conditions become:

$$y_1 = 0,\ y_2 = 1,\ y_4 = 0,\ y_6 = 1,\ y_8 = 1, \text{at}\ \eta = 0, \\ y_2 = 0,\ y_4 = 0,\ y_6 = 0,\ y_8 = 0,\ \text{at}\ \eta \to \infty. \tag{31}$$

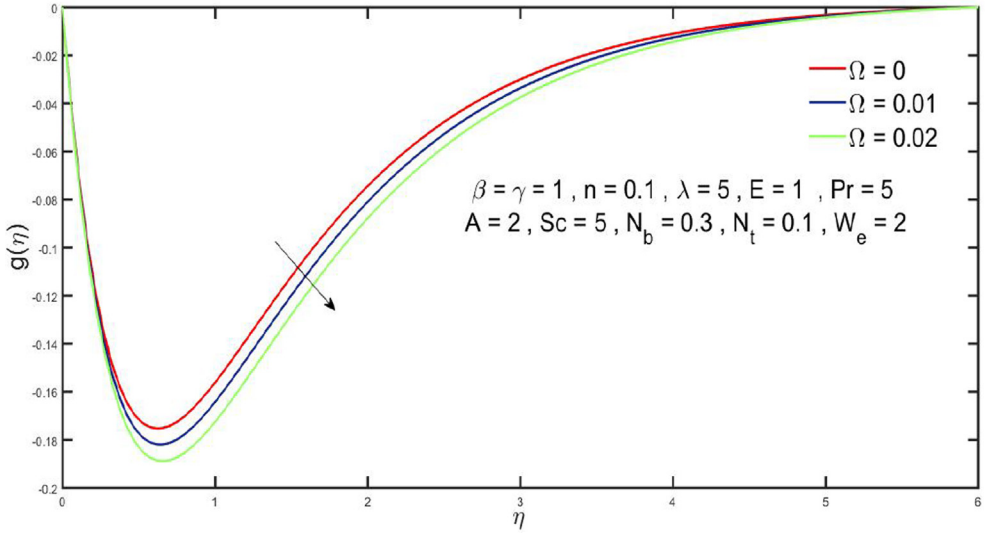


**Fig 9** Effects of Ω on $g(\eta)$.

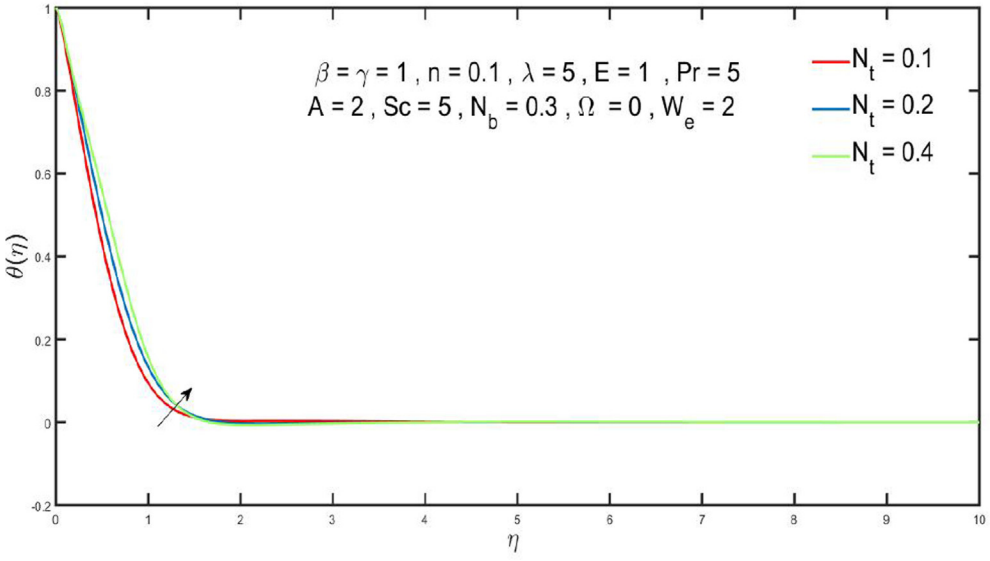


**Fig 10** Impact of $N_t$ on $\theta(\eta)$.

The Eqs. (26)–(30) with Eq. (31) are solved by using bvp4c matlab software. Having tolerance $10^{-6}$ and take step size 0.001.

## 4. Results and discussion

In current section we will investigate the physical behavior of distinct parameters such as variable viscosity parameter $A$, rotational parameter $\Omega$, thermophoresis parameter $N_t$, Weissengnberg number $We$ Schmidt number Sc, mixed convection parameters $\beta$, Prandtl number Pr, chemical reaction rate constant $\lambda$, power law of index $n$ and buoyancy parameter $\gamma$ on velocity components ($g(\eta)$ and $f'(\eta)$, temperature e distribution $\theta(\eta)$ and concentration profile $\varphi(\eta)$. Fig. 2 reveals that the velocity $f'(\eta)$is affected by viscosity parameter $A$ . The velocity of the liquid dwindles by increasing parameter $A$. Since the variable viscosity isproportional to cohesive force and adhesive force. So the cohesive force and adhesive force rise the liquid resistance by raising density of molecules consequently the velocity of the liquid reduces. Fig. 3 examines that increasing the Weissenberg number $We$ yields slightly decline in $f'(\eta)$and boundary layer. Rise in the parameter $We$ increases relaxation time, it can reveal that the liquid requires further resistance to flow and the velocity minorly decrease. Fig. 4 exhibits the significance of power law index parameter $n$ relative to f'(η), as tangent hyperbolic is a shear thinning fluid ($n < 1$), so increasing values of $n$ dwindles f'(η). Fig. 5 contemplates the behavior of parameter $\beta$ on f'(η). Raising values of $\beta$ increase the f'(η). The mix convection parameter $\beta$ is ratio of buoyancy to inertial forces. By increase in convection parameter $\beta$ the buoy-

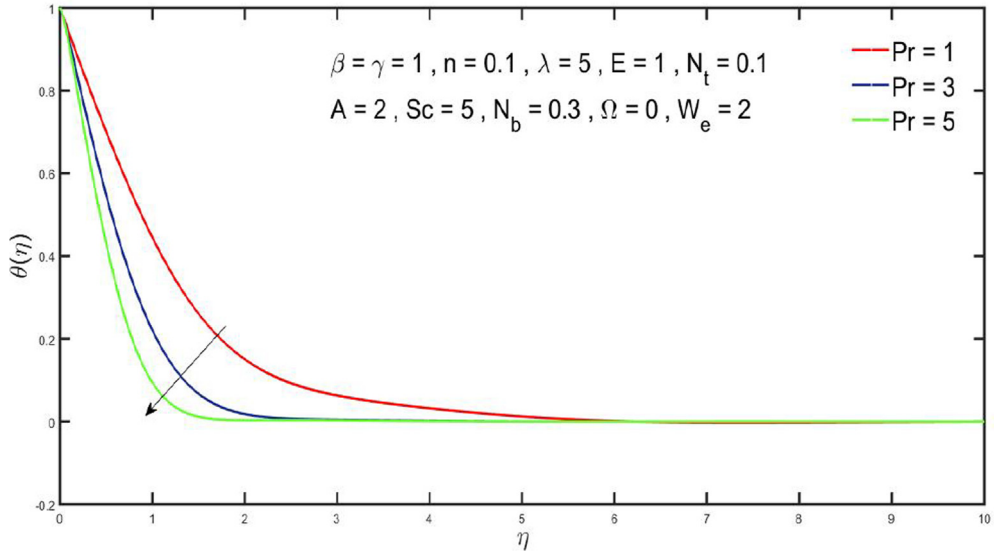


**Fig 11** Impact of Pr on.$\theta(\eta)$.

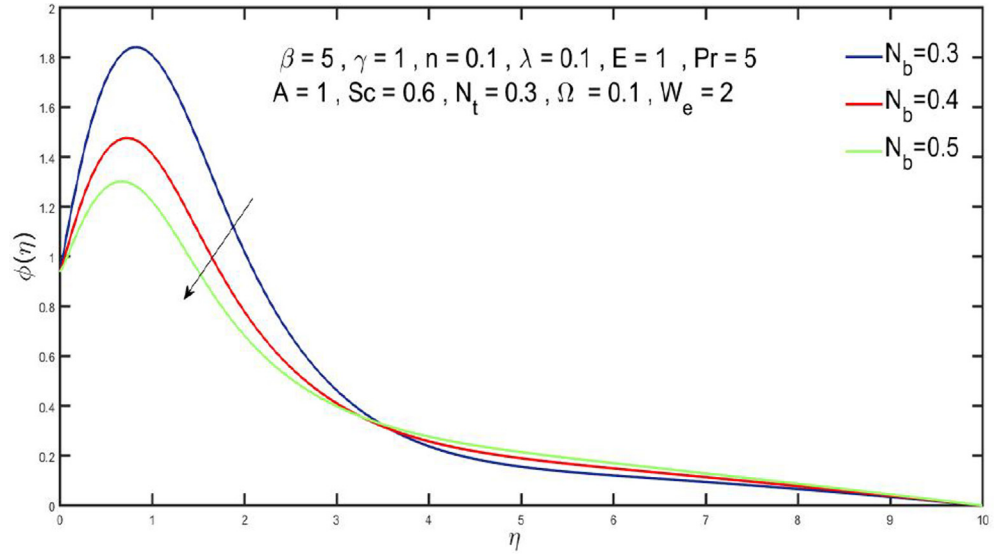


**Fig 12** Impact of $N_b$ on $\varphi(\eta)$.

ancy forces preeminent the inertia forces which rises the f'(η). The significance of the buoyancy parameter $\gamma$ on $f'(\eta)$ is presented in the Fig. 6. It declares that $f'(\eta)$ raises when $\gamma$ increases. Physically the buoyancy force increases by large $\gamma$ whose velocity is higher. Fig. 7 illustrates that $g(\eta)$ is affected by viscosity parameter A. The velocity of the liquid decreases by increasing viscosity parameter $A$. Since the variable viscosity is proportional to cohesive and adhesive forces. The cohesive and adhesive forces raise the liquid resistance by raising density of molecule. Fig. 8 examines increasing the Weissenberg number $We$ yield slightly decline in $g(\eta)$ and boundary layer. The raise in parameter $We$ also raises relaxation time, it can be revealed that the liquid requires further resistance to flow and the velocity $g(\eta)$ minorly decreases. Fig. 9 examines the role of for the distinct values of parameter Ω. It is believed that the parameter Ω plays significant character in accelerating the flow in $y$-direction. Due to increase in the parameter Ω the oscillatory movement in the $g(\eta)$ increases. Fig. 10 represents the significance of $N_t$ on temperature distribution $\theta(\eta)$. Increase in $N_t$ leads greater temperature profile $\theta(\eta)$ and thermal thickness, due to which nanoparticles have a strong thermophoresis force against temperature gradient. It is due to the cold cover that the nanoparticles move, which increases the thickness of the thermal layer. Fig. 11 shows the relationship between temperature $\theta(\eta)$ and $\eta$ for distinct values of Pr number. By raising values of Pr number, the thermal conductivity and thermal layer thickness decreases. Because thermal diffusion and Pr number have inverse relation. Fig. 12 delineates the significance of solutal profile $\varphi(\eta)$ on Brownian motion $N_b$ . The higher Brownian motion $N_b$ dwindles as the contact between molecules increase. Since Brownian motion $N_b$uses

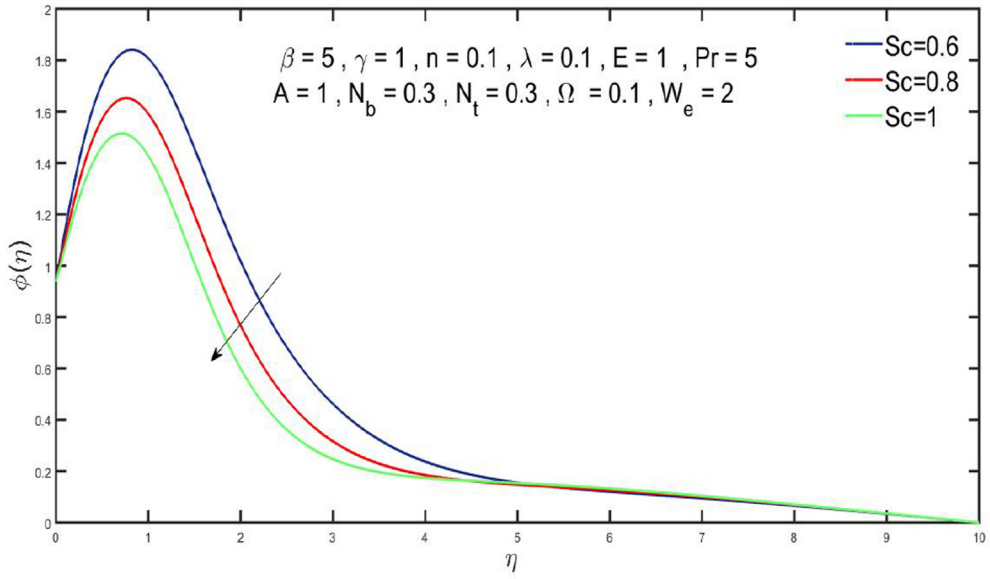


**Fig 13** Impact of $Sc$ on $\varphi(\eta)$.

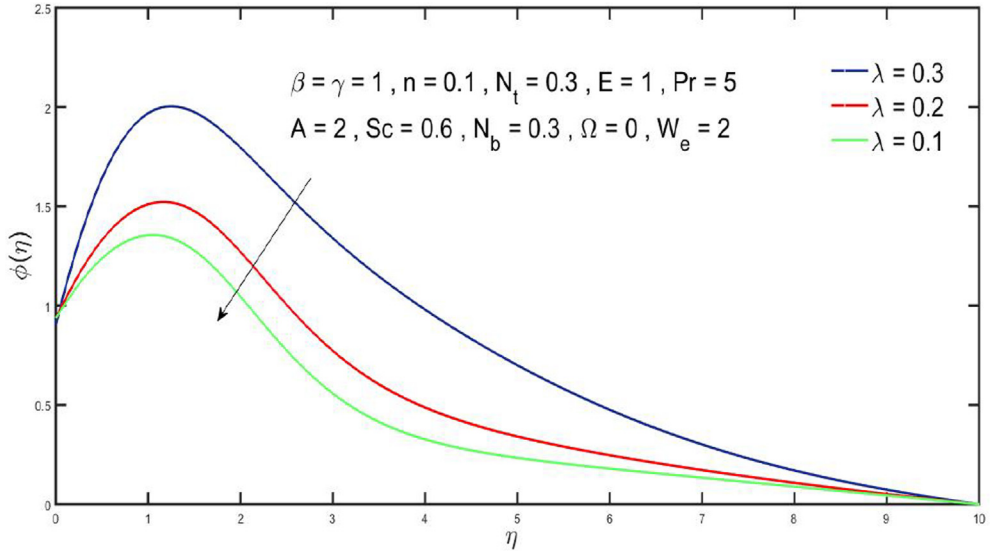


**Fig 14** Impact of λ on $\varphi(\eta)$.

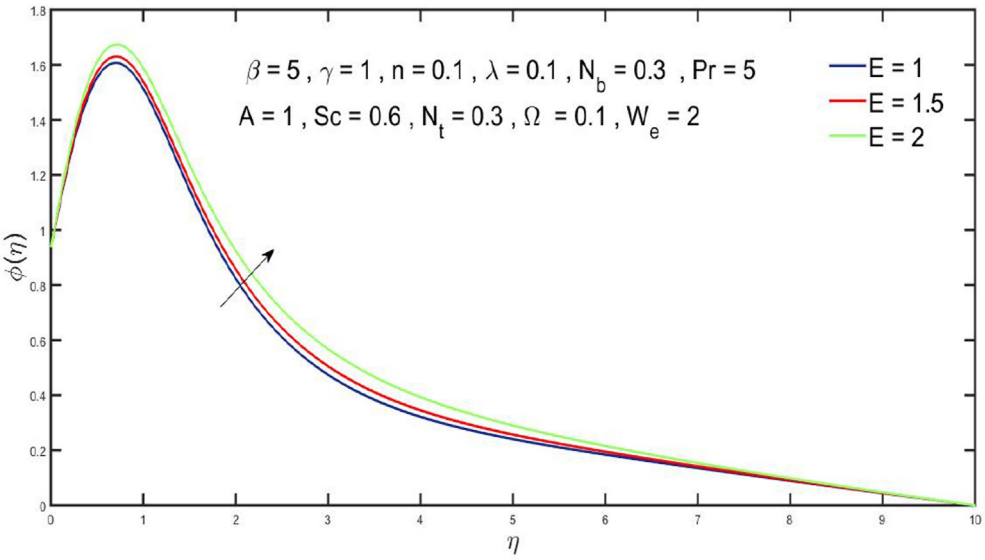


**Fig 15** Impact of E on $\varphi(\eta)$.

**Table 1**

Numerical data of $-Re_x^{\frac{1}{2}} C_f$ and $-Re_y^{\frac{1}{2}} C_f$ for different values of $A$, $\beta$ , $We$, $n$ , $\gamma$ and $\Omega$.

| $A$ | $n$ | $We$ | $\beta$ | $\gamma$ | $\Omega$ | $-Re_x^{\frac{1}{2}} C_f$ | $-Re_y^{\frac{1}{2}} C_f$ |
|---|---|---|---|---|---|---|---|
| -0.4 | 0.3 | 0.2 | 0.3 | 0.4 | 0.2 | 1.4787 | 0.3935 |
| -0.3 | | | | | | 1.4244 | 0.3844 |
| -0.2 | | | | | | 1.4154 | 0.3673 |
| -0.1 | | | | | | 1.2975 | 0.3367 |
| -0.1 | 0.3 | 0.2 | 0.3 | 0.4 | 0.2 | 1.2975 | 0.3367 |
| | 0.5 | | | | | 1.0098 | 0.3640 |
| | 0.6 | | | | | 0.8536 | 0.3829 |
| | 0.7 | | | | | 0.6734 | 0.4012 |
| -0.1 | 0.3 | 0.2 | 0.3 | 0.4 | 0.2 | 1.2975 | 0.3367 |
| | | 0.3 | | | | 1.3479 | 0.3984 |
| | | 0.4 | | | | 1.3992 | 0.4640 |
| | | 0.6 | | | | 1.5010 | 0.6063 |
| -0.1 | 0.3 | 0.2 | 0.3 | 0.4 | 0.2 | 1.2975 | 0.3367 |
| | | | 0.4 | | | 1.3418 | 0.3352 |
| | | | 0.6 | | | 1.4334 | 0.3318 |
| | | | 0.7 | | | 1.4808 | 0.3299 |
| -0.1 | 0.3 | 0.2 | 0.3 | 0.4 | 0.2 | 1.2975 | 0.3367 |
| | | | | 0.5 | | 1.3472 | 0.3346 |
| | | | | 0.7 | | 1.4494 | 0.3303 |
| | | | | 0.9 | | 1.5557 | 0.3254 |
| -0.1 | 0.3 | 0.2 | 0.3 | 0.4 | 0.2 | 1.2975 | 0.3367 |
| | | | | | 0.3 | 1.2409 | 0.4735 |
| | | | | | 0.4 | 1.1552 | 0.6287 |
| | | | | | 0.5 | 1.0338 | 0.8112 |

such force to separate the molecules in opposite direction of solutal gradient. The significance of the $Sc$on $\varphi(\eta)$ presented in Fig. 13 It has been shown that the raising values of $Sc$ decreases the profile $\varphi(\eta)$ . Physically $Sc$ is based on the Brownian diffusivity. The rise in Schmidt number $Sc$ reduces the Brownian diffusion. Fig. 14 has been compiled to illustrate the significance of reaction parameter $\lambda$on concentration distribution $\varphi(\eta)$ . It is seen that concentration profile reduces due

**Table 2**

Numerical data of $(Re_x)^{-\frac{1}{2}}Nu_x$ for different values of $N_t$, $Sc$, $N_b$ and $Pr$ .

| $Pr$ | $N_t$ | $N_b$ | $Sc$ | $(Re_x)^{-\frac{1}{2}}Nu_x$ |
|---|---|---|---|---|
| 0.9 | 0.2 | 0.2 | 2 | 0.5740 |
| 1.5 | | | | 0.6220 |
| 2.5 | | | | 0.6980 |
| 3.5 | | | | 0.7602 |
| 3.5 | 0.2 | 0.2 | 2 | 0.7602 |
| | 0.3 | | | 0.6681 |
| | 0.5 | | | 0.5023 |
| | 0.6 | | | 0.4306 |
| 3.5 | 0.2 | 0.2 | 2 | 0.7602 |
| | | 0.3 | | 0.6587 |
| | | 0.4 | | 0.5639 |
| | | 0.5 | | 0.4778 |
| 3.5 | 0.2 | 0.2 | 2 | 0.7602 |
| | | | 3 | 0.7446 |
| | | | 4 | 0.7236 |
| | | | 5 | 0.7011 |

**Table 3**

Numerical data of $(Re_x)^{-\frac{1}{2}}Sh_x$ for distinct values of $N_b$, $\gamma$, $Sc$, $\lambda$ and $\theta_r$.

| $\lambda$ | $N_b$ | $Sc$ | $\gamma$ | $(Re_x)^{-\frac{1}{2}}Sh_x$ |
|---|---|---|---|---|
| 0.1 | 0.2 | 0.1 | 0.4 | 0.4339 |
| 0.3 | | | | 0.4248 |
| 0.4 | | | | 0.4158 |
| 0.5 | | | | 0.4042 |
| 0.5 | 0.2 | 0.1 | 0.4 | 0.4339 |
| | 0.3 | | | 0.4498 |
| | 0.4 | | | 0.4723 |
| | 0.5 | | | 0.4855 |
| 0.5 | 0.2 | 0.1 | 0.4 | 0.4339 |
| | | 1 | | 0.2937 |
| | | 2 | | 0.2121 |
| | | 3 | | 0.1887 |
| 0.5 | 0.2 | 0.1 | 0.4 | 0.4339 |
| | | | 0.9 | 0.4047 |
| | | | 2 | 0.3588 |
| | | | 2.5 | 0.2966 |

**Table 4**

Numerical results for wall slopes f''(0) and g'(0) for various values of **Ω.**

| Ω | $f''(0)$ | $g'(0)$ | $f''(0)$ | $g'(0)$ | $f''(0)$ | $g'(0)$ |
|---|---|---|---|---|---|---|
| | Javed et al. [36] | | Mustafa et al. [37] | | Present | |
| 0.2 | -1.3474169 | -0.37015223 | -1.3474203 | -0.3701525 | -1.3474189 | -0.3701424 |
| 0.5 | -1.5194131 | -0.76251409 | -1.5194195 | -0.7625142 | -1.5193125 | -0.7624140 |
| 1.0 | -1.8024646 | -1.2179575 | -1.8024749 | -1.2179573 | -1.8025699 | -1.2179585 |
| 2.0 | -2.2827968 | -1.8485044 | -2.2828127 | -1.8485032 | -2.2829095 | -1.8486011 |
| 5.0 | -3.3444338 | -3.0609192 | -3.3444611 | -3.0609164 | -3.3443128 | -3.06092190 |
| 10.0 | -4.6017220 | -4.390640 | -4.6017619 | -4.399058 | -4.6018520 | -4.399110 |

to decline in reaction parameter $\lambda$.Fig. 15 presents effect of the activation energy $E$ on dimensionless $\varphi(\eta)$. This eventually leads to the chemical which increases the concentration of nanoparticles. The numerical values are exhibited by drawing tables of skin friction, Nusselt number and Sherwood number. Table 1 expresses the values of $-Re_x^{\frac{1}{2}}C_f$ and $-Re_y^{\frac{1}{2}}C_f$ by increasing distinct values of viscosity parameter $A$, whereas other parameters such as $n$, $We$, $\beta$, $\gamma$ and Ω are constant. It is seen that the coefficient of the skin friction $-Re_x^{\frac{1}{2}}C_f$ has large impact by increasing viscosity parameter, Weissengberg number $e$ , mixed convection parameter $\beta$ and buoyancy force parameter $\gamma$. The coefficient of skin friction $-Re_y^{\frac{1}{2}}C_f$ decreases by raising values of viscosity parameter $A$, mixed convection parameter $\beta$ and buoyancy force parameter $\gamma$. Tables 2 and 3 express the values of $(Re_x)^{-\frac{1}{2}}Nu_x$ and $(Re_x)^{-\frac{1}{2}}Nu_x$ for distinct parameters. It has been examined that $(Re_x)^{-\frac{1}{2}}Nu_x$ and $(Re_x)^{-\frac{1}{2}}Nu_x$ has less values by raising the parameter $Sc$and Brownian parameter $N_b$. The values of drag coefficients at the surface $f''(0)$ and $g'(0)$ corresponding to different values of rotational parameter Ω are contained in Table 4. Present results are consistent with the results of Javed et al. (Khan et al., 2014) and Mustafa et al. (Nehad Ali Shah).

## 5. Conclusion

This paper is concerned with the significance of 3D shear thinning fluid flow over a stretchable rotatory surface along with mixed convention, variable viscosity and heat generation. The non-linear equations are solved numerically by BVP4C Matlab package. The main remarks of present discussion for numerous physical parameters are listed below:

- Concentration distribution has decreasing trend relative to higher values of Schmidt number $Sc$ and Prandtl number Pr.
- Velocity profile declines for increasing rotational parameter Ω and power law index $n$.
- Higher values of mixed convection parameter $\beta$ and Buoyancy parameter $\gamma$ improves the velocity distribution.
- Greater values of $A$ and $We$ reduces the surface force while it exhibits same behavior for $f'(\eta)$.
- Concentration profile has diminishing trend for reaction parameter.
- Temperature profiles are enhancing for thermophoresis parameter $N_t$while concentration profile reduces for Brownian motion parameter $N_t$.
- Concentration distribution rises with increasing activation energy.
- Higher values of Pr showing decline behavior for temperature profile.

## Declaration of Competing Interest

The authors declare that they have no known competing financial interests or personal relationships that could have appeared to influence the work reported in this paper.

## References

O.A. Abegunrin, I.L. Animasaun, Motion of Williamson fluid over an upper horizontal surface of a paraboloid of revolution due to partial slip and buoyancy: boundary layer analysis, doi:10.4028/www.scientific.net/DDF.378.16 c 2017.

Abegunrin, O.A., Okhuevbie, S.O., Animasaun, I.L., 2016. Comparison between the flow of two non-Newtonian fluids over an upper horizontal surface of paraboloid of revolution: boundary layer analysis. Alex. Eng. J. 55, 1915–1929.

Ahmad, I., Sajid, M., Awan, W., Rafique, M., Aziz, W., Ahmed, M., Abbasi, A., Taj, M., 2014. MHD flow of a viscous fluid over an exponentially stretching sheet in a porous medium. J. Appl. Math. 256761.

Ali, A., Akhtar, J., Anjum, H.J., Awais, M., Shah, Z., Kumam, P., 2021. 3D nanofluid flow over exponentially expanding surface of Oldroyd-B fluid. Ain Shams Eng. J. 12 (4), 3939–3946.

Amahmid, A., Hasnaoui, M., Mamou, M., Vasseur, P., 1999. Boundary layer flows in a vertical porous enclosure induced by opposing buoyancy forces. Int. J. Heat Mass Transf. 42, 3599–3608.

Animasaun, I.L., Mahanthesh, B., Sarojamma, G., Damisa, J.S., 2020. Significance of thickness of paraboloid of revolution and buoyancy

forces on the dynamics of Erying-Powell fluid subject to equal diffusivity kind of quartic autocatalysis. Phys. A 549, 124047.
Animasauna, I.L., Ibraheema, R.O., Mahanthesh, B., Babatunde, H. A., 2019. A metaanalysis on the effects of haphazard motion of tiny/nanosized particles on the dynamics and other physical properties of some fluids. Chin. J. Phys. 60, 676–687.
Atif, S.M., Hussain, S., Sagheer, M., 2019. Effect of viscous dissipation and Joule heating on MHD radiative tangent hyperbolic nanofluid with convective and slip condition. J. Braz. Soc. Mech. Sci. Eng. 41, 189.
Bashir, M.F.M., Mabood, F., Satya Narayana, P.V., Venkateswarlu, B., Ismail, M.I.M., 2022. Significance of viscous dissipation on the dynamics of ethylene glycol conveying diamond and silica nanoparticles through a diverging and converging channel. J. Therm. Anal. Calorim. 147, 661–674.
Bellahsen, M.-N., Husson, L., Autin, J., Leroy, S., d'Acremont, E., 2013. The effect of thermal weakening and buoyancy forces on rift localization: field evidences from the Gulf of Aden oblique rifting. Tectonophysics 607, 80–97.
M.M. Bhatti, A. Zeeshan, R. Ellahi, 2016. Heat transfer analysis on peristaltically induced motion of particle-uid suspension with variable viscosity: clot blood model, computer methods and programs in biomedicine, 137 115–124.
Chang, S.W., Liou, T.M., Po, Y., 2010. Coriolis and rotating buoyancy effect on detailed heat transfer distributions in a two-pass square channel roughened by 45 ribs at high rotation numbers. Int. J. Heat Mass Transfer 53, 1349–1363.
Chernyak, V.G., Sograbi, T.V., 2019. The role of molecule-surface interaction in thermophoresis of an aerosol particle. J. Aerosol. Sci. 128, 62–71.
D. Petrolo, L. Chiapponi, S. Longo, M. Celli, A. Barletta and V. Di Federico, Onset of Darcy–Benard convection under throughflow of a shear-thinning fluid, https://doi.org/10.1017/jfm.2020.84.
Dogonchi, A.S., Seyyedi, S.M., Hashemi-Tilehnoee, M., Chamkha, A. J., Ganji, D.D., 2019. Investigation of natural convection of magnetic nanofluid in an enclosure with a porous medium considering Brownian motion. Case Studies Thermal Eng. 14.
El-Sapa, S., 2020. Effect of permeability of Brinkman flow on thermophoresis of a particle in a spherical cavity. Eur. J. Mech./B Fluids 79, 315–323.
Gong, H., Xie, H., Liang, H., Yang, H., 2018. Combined effects of Coriolis force and temperature-viscosity dependency on hydroviscous transmission of rotating parallel disks. Tribol. Int. 117, 168–173.
Hadji, F., Ihaddadene, N., Ihaddadene, R., Betga, A., Charick, A., Logerais, P.O., 2020. Thermal conductivity of two kinds of earthen building materials formerly used in Algeria. J. Build. Eng. 32.
Hallan, P.P., Rana, N., 2001. Effect of perturbations in coriolis and centrifugal forces on the location and stability of the equilibrium point in the Robe's circular restricted three body problem. Planetary Space Sci. 49, 957–960.
R. Harish, R. Sivakumar, Effects of nanoparticle dispersion on turbulent mixed convection ows in cubical enclosure considering Brownian motion and thermophoresis, https://doi.org/10.1016/j.powtec.2020.09.054.
Hassan, A.R., 2019. Thermodynamics analysis of an internal heat generating uid of a variable viscosity reactive couette flow. J. king Saud Univ. – Sci. 31, 506–510.
Hayat, T., Riaz, A., Tanveer, A., Alsaedi, A., 2018. Peristaltic transport of tangent hyperbolic fluid with variable viscosity. Thermal Sci. Eng. Prog. 6, 217–225.
Katam, M., Ganganapalli, S., Kata, S., Rayanki, V., Satya Narayana, P.V., 2021. Coupled effect of multi-slips and activation energy in a micropolar nanoliquid on a convectively heated elongated surface. Heat Transfer 50 (6), 6237–6258.
Khan, J.A., Mustafa, M., Hayat, T., Farooq, M.A., Alsaedi, A., Liao, S.J., 2014. On model for three-dimensional flow of nanofluid: An application to solar energy. J. Mol. Liquid 194, 41–47.
Khan, J.A., Mustafa, M., Hayat, T., Sheikholeslami, M., Alseadi, A., 2015. Three-Dimensional flow of nanofluid induced by an exponentially stretching sheet: an application to solar energy. PLoS One 10 (3), 0116603.
Khan, M.N., Nadeem, S., 2021. A comparative study between linear and exponential stretching sheet with double stratification of a rotating Maxwell nanofuid flow. Surf. Interfaces 22, 100886.
Khan, M., Salahuddin, T., Malik, M.Y., Mallawi, F.O., 2018. Change in viscosity of Williamson nanofluid flow due to thermal and solutal stratification. Int. J. Heat Mass Transfer 126, 941–948.
Mittal, A.S., Patel, H.R., 2020. Influence of thermophoresis and Brownian motion on mixed convection two dimensional MHD Casson fluid flow with non-linear radiation and heat generation. Physica A 537, 122710.
M. Mustafa, M. Wasim, T. Hayat, A. Alsaed, A revised model to study the rotating flow of nanofluid over an exponentially deforming sheet: Numerical solution, https://doi.org/10.1016/j.molliq.2016.11.078.
Nadeem, S., Akbar, N.S., Hameed, M., 2010. Peristaltic transport and heat transfer of a MHD Newtonian áuid with variable viscosity. Int. J. Numerical Methods Fluids 63, 1375–1393.
Nagendramma, V., Leelarathnam, A., Raju, C.S.K., Shehzad, S.A., Hussain, T., 2018. Doubly stratied MHD tangent hyperbolic nanouid flow due to permeable stretched cylinder. Results Phys. 9, 23–32.
Naidu, K.K., Babu, D.H., Reddy, S.H., Satya Narayana, P.V., 2021. Radiation and Partial Slip Effects on Magnetohydrodynamic Jeffrey Nanofluid Containing Gyrotactic Microorganisms Over a Stretching Surface. Journal of Thermal Analysis and Engineering Applications 13, (1) 031011.
Shah, N.A., Animasaun, I.L., Ibraheem, R.O., Babatunde, H.A., Sandeep, N., Pop, I., Scrutinization of the effects of Grashof number on the flow of different fluids driven by convection over various surface, 10.1016/j.molliq.2017.11.04.
Pei, B., Yong, X., Jiang-Lun, W., 2020. Stochastic averaging for stochastic differential equations driven by fractional Brownian motion and standard Brownian motion. Appl. Math. Lett. 100, 106006.
Ramachandran, S., Sobhan, C.B., Peterson, G.P., 2020. Thermophoresis of nanoparticles in liquids. Int. J. Heat Mass Transf. 147, 118925.
Riahi, D.N., 2001. Effects of centrifugal and coriolis forces on a hydromagnetic chimney convection in a mushy layer. J. Crystal Growth 226, 393–405. 18.
Salahuddin, T., Malik, M.Y., Hussain, A., Awais, M., Khan, I., Khan, M., 2017. Analysis of tangent hyperbolic nanofluid impinging on a stretching cylinder near the stagnation point. Results Phys., 426–434
Salahuddin, T., Muhammad, S., Sakinder, S., 2019. Impact of generalized heat and mass flux models on Darcy- Forchheimer Williamson nanofluid flow with variable viscosity. Physica scripta 94, 125–201.
Satya Narayana, P.V., Tarakaramu, N., Sarojamma, G., Animasaun, I.L., 2021. Numerical simulation of nonlinear thermal radiation on the 3D flow of a couple stress Casson nanofluid due to a stretching sheet. J. Thermal Anal. Eng. Appl. 13, (2) 021028.
Satya Narayana, P.V., Tarakaramu, N., Babu, D.H., 2021. Influence of chemical reaction on MHD couple stress nanoliquid flow over a bidirectional stretched sheet. Int. J. Ambient Energy. https://doi.org/10.1080/01430750.2021.1923569.
Shah, Z., Gul, T., Islam, S., Khan, M.A., Bonyah, E., Hussain, F., Mukhtar, S., Ullah, M., 2018. Three dimensional third grade nanofluid flow in a rotating system between parallel plates with Brownian motion and thermophoresis effects. Results Phys. 10, 36–45.
Shahzad, F., Sagheer, M., Hussain, S., 2019. MHD tangent hyperbolic nanofuid with chemical reaction, viscous dissipation and Joule heating effects. AIP Adv. 9, 025007.

Shamshuddin, M.D., Satya Narayana, P.V., 2020. Combined effect of viscous dissipation and Joule heating on MHD flow past a Riga plate with Cattaneo-Christov heat flux. Indian J. Phys. 94, 1385–1395.

Ullah, I., Shafie, S., Khan, I., Hsiao, K.L., 2018. Brownian diffusion and thermophoresis mechanisms in Casson fluid over a moving wedge. Results Phys. 9, 183–194.

Ullah, Z., Zaman, G., Ishak, A., 2020. Magnetohydrodynamic tangent hyperbolic fluid flow past a stretching sheet. Chin. J. Phys. 66, 258–268.

Venkateswarlu, B., Satya Narayana, P.V., 2021. Cu-$Al_2O_3/H_2O$ hybrid nanofluid flow past a porous stretching sheet due to temperatue-dependent viscosity and viscous dissipation. Heat Transfer 50 (1), 432–449.

Wakif A., Animasaun I. L., Satya Narayana P. V. and Sarojamma G., Meta-analysis on thermo-migration of tiny/nano-sized particles in the motion of various fluids, https://doi.org/10.1016/j.cjph.2019.12.002.

Wakif, A., Animasaun, I.L., Satya Narayana, P.V., Sarojamma, G., 2020. Meta-analysis on thermo-migration of tiny/nano-sized particles in the motion of various fluids. Chin. J. Phys. 68, 293–307.

Wang, F., Ahmed, S., Al Mdallal, Q., Alammari, M., Khan, M.N., Rehman, A., 2022. Natural bio–convective flow of Maxwell nanofuid over an exponentially stretching surface with slip effect and convective boundary condition. Sci. Rep. 12, 2220.

Wang, K., Su, X., Li, Z., Wu, S., Zhou, W., Wang, R., Chen, S., Wang, X., 2020. Generation of non-Kolmogorov atmospheric turbulence phase screen using intrinsic embedding fractional Brownian motion method. Optik – Int. J. Light Electron Optics 207.